Shadows

David K. Lynch

Thule Scientific, P.O. Box 953, Topanga, California 90290, USA (thule@earthlink.net)

Received 18 July 2014; revised 6 November 2014; accepted 7 November 2014;
posted 10 November 2014 (Doc. ID 217186); published 7 January 2015

We investigate the brightness distribution in and around outdoor shadows (for a variety of sky conditions) using modeling and field measurements. The dominant factor influencing the brightness of a shadow is the solid angle subtended by the object blocking the Sun. Occulters at the zenith that subtend a small solid angle cast shadows that are bright and possess a nearly uniform brightness across their extent. Shadows from large occulters are much darker and their brightness varies considerably, being darkest at their centers. For nonzenith occulters, the proximal (nearest the Sun) side of the shadow is darker than the distal side and the shadow will be darkest beneath the center of the occulter. Occulters (e.g., tree or cloud) influence the brightness of sunlit portions near the shadow because they block part of the sky and reflect light into the shadow. The aureole has a significant influence on the brightness of shadow edges. Semi-analytic formulations for the brightness in shadows are presented, and analytic expressions in wells and tunnels are derived.

OCIS codes: (080.0080) Geometric optics; (010.1290) Atmospheric optics; (010.7295) Visibility and imaging; (330.0330) Vision, color, and visual optics.

http://dx.doi.org/10.1364/AO.54.00B154

1. Introduction

Shadows are so familiar that their explanation might seem obvious, perhaps trivial. But this is not the case. For example, Fig. 1 shows a number of interesting shadow effects from a coffee mug casting its shadow on white paper. The shadow is blue because in the absence of direct sunlight only blue skylight is illuminating it. The shadow is darker near the mug and becomes brighter away from it. An observer standing on the paper near the mug would see the mug subtending a large solid angle which blocks much of the skylight. The mug's solid angle decreases as the observer moves away from it. As a result, the mug blocks less skylight (causing the shadow to grow brighter). Perhaps surprisingly, the presence of the mug also affects the sunlit portion of the paper by blocking part of the sky. As the observer moves away from the mug's shadow, the sunlit portions brighten. Thus, from a simple observation we discover a fundamental truth: an occulting object influences the entire scene's brightness, not just in its own shadow.

Another example occurs on overcast days (Fig. 2). With no direct sunlight but only light scattered through clouds, the illumination source is the overcast itself. The shadow is diffuse but still present. Since the light is coming from all directions, the shadow is also cast in all directions. These shadows are darkest at their centers where the occulter subtends the largest solid angle and consequently blocks the largest amount of the skylight.

Shadows display wide variations due to the illumination circumstances: clear skies, partly cloudy and overcast skies, nearby landscape objects that can scatter light into shadows, the reflectivity of the surface on which they fall, size of the occulting object relative to its height above ground height, and so on.

Shadows are fundamentally volumetric phenomena; i.e., they exist in three dimensions, not just as a dark spot on the ground. Artists and computer scene generators classify them into three categories [1]: form, space, and cast. In Fig. 1, form shadows are on the body casting the shadow (in this case, the side of the mug without direct solar illumination)

1559-128X/15/04B154-11$15.00/0

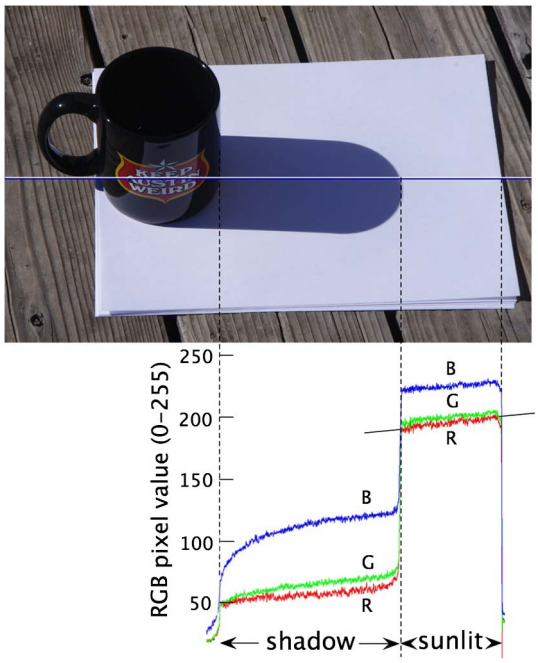

Fig. 1. RGB scans through the photograph along the horizontal line indicated. With increasing distance from the mug the shadow grows brighter because the mug is blocking less skylight; i.e., the mug is subtending a smaller solid angle. The effect is also evident in the sunlit portion of the scene. Note that the shadow was also blue because only blue sky light could reach it. The Sun was relatively low and dim, so the sunlit white paper was similarly blue. Digital single lens reflex camera was used to take the photograph. RGB scans were retrieved using Igor Pro software. Scans were boxcar averaged by three pixels to reduce noise.

and facing the cast shadow. It is hard to see in Fig. 1 because the mug is so dark. The space shadow occupies the volume of shadowed space between the mug and the paper. It is invisible here because there is nothing (like smoke or haze) to scatter light from

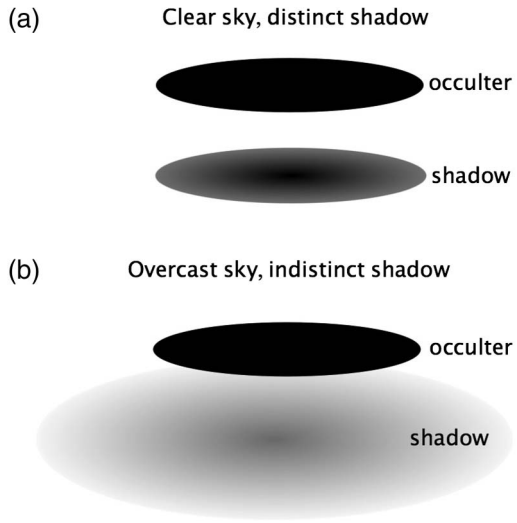

Fig. 2. (a) On clear days the shadow has sharp edges (penumbral effects ignored). (b) On overcast days the shadow has no edges because the illumination source (the clouds) covers the entire celestial hemisphere.

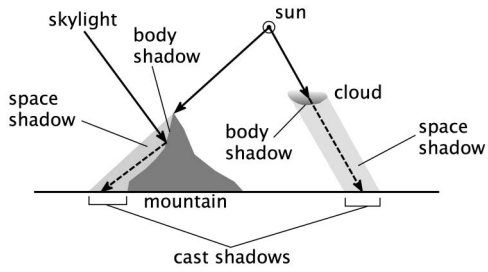

Fig. 3. There are three kinds of shadows: (a) body shadow on the shady side of the occulting object, (b) space shadow that is normally invisible, and (c) the cast shadow on the ground, the one we usually think of as the shadow. Light can reach the cast shadow from the sky and the body shadow.

the volume, as there is in the case of crepuscular rays or an eclipsed moon. The cast shadow is seen on the ground and is the shadow we most often think of. Note that an occulter blocks skylight, but it can also add illumination to the shadow (Fig. 3). A good example is a cloud whose form shadow is never black because light emerges from the cloud's shaded underside. Another example is a mountain. Its form shadow will reflect skylight into the cast shadow. Scene modelers are well aware of such effects [2–4].

Shadows have been previously studied for a wide variety of applications [5–7]. Yet few if any investigators have reported or clearly stated some of the most fundamental aspects of shadows. In this paper, we hope to provide a foundation for understanding shadows by theoretically deriving some of their basic properties and demonstrating them with measurements, primarily in the outdoor landscape. We have analyzed shadows using geometrical optics and realistic illumination sources. Only umbral shadows were considered, requiring that all occulters subtend solid angles much greater than that of the Sun ($\sim 6 \times 10^{-5}$ str). We treat the Sun as a point source and ignore diffraction (and solar limb darkening). We will also ignore the intrinsic color of the sky and also the properties of the surface upon which the shadow is cast which we will assume to be uniform and neutral in color.

2. Theory: Shadows from Occulters at the Zenith

A. Brightness at the Center of a Shadow

We begin with the simplest case (Fig. 4): a shadow cast on the ground from an occulting object at the zenith that blocks the Sun, also at the zenith. The ideal occulter would be an infinitely thin, circular, horizontally oriented, opaque black disk. Such a disk would not reflect light back to the atmosphere to be further scattered, nor would it reflect ground light from its underside (back into the shadow).

Let the occulter have a diameter w and a height h above the ground. At the center of the shadow on the ground, the occulter blocks a solid angle of

$$\Omega = 2\pi(1 - \cos\,\theta_0), \tag{1}$$

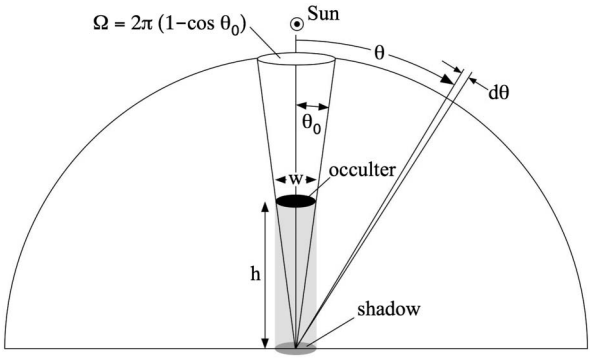

Fig. 4. Geometry of a shadow cast by the zenith sun. The nonreflective opaque circular occulter (with diameter w and height h above the ground) casts a circular shadow. Seen from the ground, the occulter subtends a solid angle Ω with angular radius θ_0.

where the zenith angle of the occulter's edge θ_0 is given by

$$\theta_0 = \tan^{-1}(w/2h). \tag{2}$$

The brightness at the center of the shadow I_S can be calculated by integrating over the entire 2π sr of sky light I_A, then subtracting from it the contribution from the sky blocked by the occulter I_B, with a solid angle Ω. The assumption here is that the brightness of the shadow is proportional to the amount of skylight reaching it. We shall initially adopt a normalized, dimensionless sky radiance B_A that is proportional to air mass and is of the form

$$B_A(\theta) = \sec\,\theta, \tag{3}$$

which gives a unit brightness at the zenith and is a good approximation for a plane-parallel, optically thin atmosphere until we approach roughly $\theta > 75°$. Equation (3) implicitly assumes that the atmosphere is composed of particles that scatter light isotropically. At any given zenith distance, light reaching the surface will be diluted (per unit area on the ground) by a factor of cos θ. Taking these terms into account, the differential brightness contribution of the sky to the shadow is

$$dI_A = \sec\,\theta\, 2\pi\,\sin\,\theta d\theta\,\cos\,\theta = 2\pi\,\sin\,\theta d\theta. \tag{4}$$

Here, sec θ cancels cos θ, and we revert to a situation where calculating irradiance has simply become one of computing solid angles. Integrating θ from 0 to $\pi/2$, we find

$$I_A = 2\pi \int_0^{\pi/2} \sin\,\theta \mathrm{d}\theta = 2\pi, \tag{5}$$

which is a convenient value for the relative whole sky irradiance (in steradians) that is falling on the center of the shadow. From this, we must subtract I_B (radiance from the sky around the zenith, blocked by the occulter). It is the same functional form as Eq. (5), except the integration limits are 0 to θ_0,

$$I_B = 2\pi \int_0^{\theta_0} \sin\,\theta \mathrm{d}\theta = 2\pi(1 - \cos\,\theta_0), \tag{6}$$

which is Eq. (1). By allowing θ_0 to go to zero, we are implicitly ignoring direct sunlight and subtracting off only that tiny portion of skylight near the zenith. In reality, θ_0 can never go to zero because when $\theta_0 < 0.25°$ (the Sun's angular radius) the Sun would be exposed leading to a penumbral shadow.

The light reaching the center of the shadow I_S is the difference between Eqs. (5) and

$$I_S = I_A - I_B = 2\pi - 2\pi(1 - \cos\,\theta_0) = 2\pi\,\cos\,\theta_0. \tag{7}$$

As expected, when θ_0 goes to zero, $I_S = 2\pi$. In the limit of very large occulters, e.g., one sitting on the ground, θ_0 goes to $\pi/2$ and I_S becomes zero, a completely dark shadow. Subtracting the two portions of the illumination from one another is like the approach taken by others [2].

We can do a similar calculation for shadows from an overcast sky by replacing sec θ with a constant brightness B_C. While not actually true, this simplifying assumption represents the starting point for more realistic overcast radiances (discussed in a subsequent paragraph) and allows an analytic solution to be obtained. Now the zenith integrals become

$$dI_A = B_C\, 2\pi\,\sin\,\theta\,\cos\,\theta \mathrm{d}\theta, \tag{8}$$

$$I_A = B_C\, 2\pi \int_0^{\pi/2} \sin\,\theta\,\cos\,\theta \mathrm{d}\theta = \pi Bc = \pi, \tag{9}$$

$$I_B = \pi B_C \sin^2\,\theta_0, \tag{10}$$

and so

$$I_S = I_A - I_B = \pi B_C \cos^2\,\theta_0. \tag{11}$$

Figure 5 shows the brightness at the center of the shadow for a clear and constant overcast sky [Eqs. (7) and (11)], normalized to unity (at $\theta_0 = 0$) for comparison. Both curves are unity at $\theta_0 = 0°$ and go to zero at $\theta_0 = 90°$. Shadows from a clear sky are relatively brighter than those from a constant overcast for every occulter size. This is because an overcast is brighter at the zenith (relative to the horizon) than is a clear sky, and it is the zenith portion I_B that is subtracted from I_A. The greatest relative difference in brightness the two curves is at $\theta_0 = 60°$, where the clear sky shadow is twice as bright as the constant overcast shadow.

To use more realistic skylight sources, we now include the differential scattering cross section for Rayleigh scattering in the clear sky calculations. For the clear sky, $B_A(\theta)$ becomes

$$B_A(\theta) = (1 + \cos^2\,\theta)\,\sec\,\theta. \tag{12}$$

Then, as before,

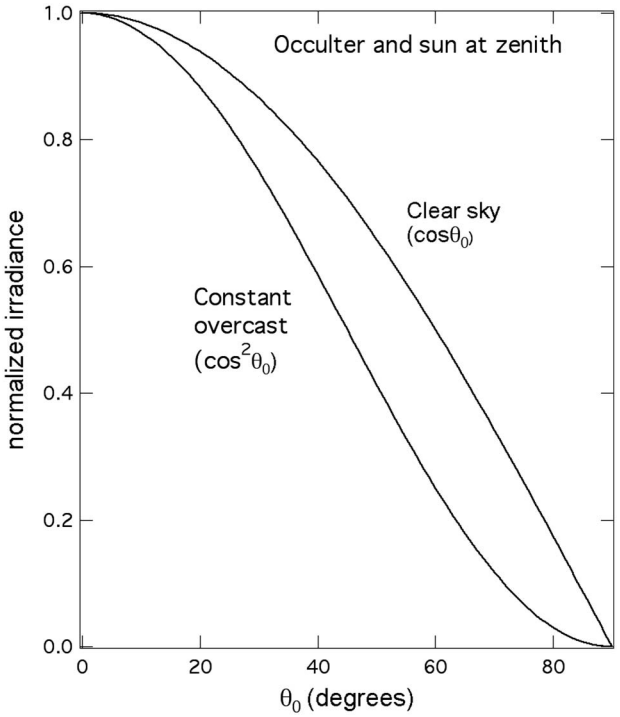

Fig. 5. Normalized comparison of the brightness of the center of the shadow (for a clear sky and overcast sky) as a function of angular radius of the occulter as would be measured from the ground [Eqs. (7) and (11)].

$$dI_A = 2\pi(1+\cos^2\theta)\sec\theta\sin\theta\cos\theta d\theta, \tag{13}$$

$$I_A = 2\pi\int_0^{\pi/2}\sin\theta d\theta + 2\pi\int_0^{\pi/2}\sin\theta\cos^2\theta d\theta = 8\pi/3. \tag{14}$$

The skylight blocked by the occulter is

$$I_B = 2\pi\int_0^{\theta_0}\sin\theta d\theta + 2\pi\int_0^{\theta_0}\sin\theta\cos^2\theta d\theta, \tag{15}$$

$$= 2\pi(1-\cos\theta_0) + 2\pi(1-\cos^3\theta_0)/3, \tag{16}$$

and therefore the shadow radiance for a Rayleigh-secant clear sky is

$$I_S = I_A - I_B$$
$$= 8\pi/3 - 2\pi(1-\cos\theta_0) - 2\pi(1-\cos^3\theta_0)/3. \tag{17}$$

For the overcast, we will use the brightness profiles of [8] for unbroken stratocumulus, shown in Fig. 6. Although brightness distributions will vary from one overcast to another [9,10], we shall take those of [8] to be representative. They can be tolerably approximated by the numerical relation

$$B_C = 24.16 - 0.001724\theta^2 \text{ W m}^{-2}\text{ sr}^{-1}, \tag{18}$$

where θ is in degrees from the zenith, also shown in Fig. 6. The constant 0.001724 has units of $\text{W m}^{-2}\text{ sr}^{-1}(\text{deg}^2)^{-1}$.

Normalizing B_C and converting to radians, we find

$$B_C = 1 - 0.23427\theta^2 = 1 - K\theta^2, \tag{19}$$

where $K = 0.23427$. The full overcast sky component is then

$$dI_A = (1-K\theta^2)2\pi\sin\theta\cos\theta d\theta$$
$$= 2\pi(\sin\theta\cos\theta d\theta - K\theta^2\sin\theta\cos\theta)d\theta, \tag{20}$$

which integrates to

$$I_A = \pi - 2\pi K[1/4\theta\sin 2\theta - 1/8(2\theta^2-1)\cos 2\theta]|_0^{\pi/2}$$
$$= \sim 2.6016. \tag{21}$$

For the occulted part of the sky reaching from the zenith to θ_0,

$$I_B = 2\pi\int_0^{\theta_0}\sin\theta\cos\theta d\theta - 2\pi K\int_0^{\theta_0}\theta^2\sin\theta\cos\theta d\theta$$
$$= 2\pi[1/2 - 1/2\cos\theta_0^2 - 1/4K\theta_0\sin(2\theta_0)$$
$$+ 1/4K\theta_0^2\cos(2\theta_0) - 1/8K\cos(2\theta_0) + K/8], \tag{22}$$

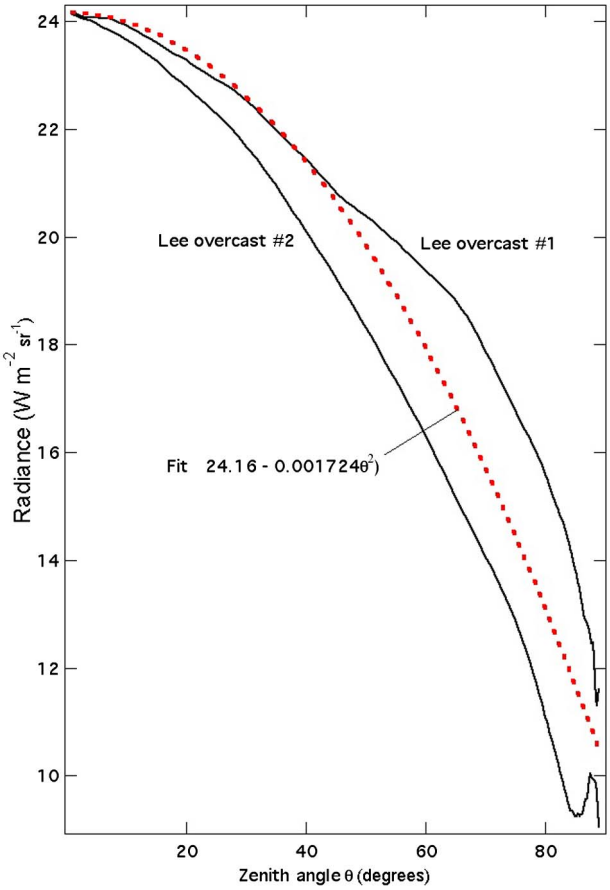

Fig. 6. Approximate fit (dotted line) to two overcasts measured by [8].

and the final expression for I_S for the shadows in [8] is then

$$I_S = I_A - I_B = \sim 2.6016 - 2\pi[1/2 - 1/2\cos\theta_0^2 - 1/4K\theta_0\sin(2\theta_0) + 1/4K\theta_0^2\cos(2\theta_0) - 1/8K\cos(2\theta_0) + K/8]. \quad (23)$$

Figure 7 shows the normalized shadow brightnesses for the Rayleigh-secant shadows [Eq. (17)], and the shadows in [8] [Eq. (23)], analogous to Fig. 5. As stated previously, the overcast shadow is fainter than the clear sky shadow, for the same reasons as explained previously for Fig. 5. Although Figs. 5 and 7 appear identical at first glance, there are subtle differences. The similarity, however, suggests that including the Rayleigh scattering term [Eq. (12)] and the overcasts of [8] [Eq. (18)] is little better than using $B_A(\theta) = \sec\theta$ for the sky [Eq. (3)] and $B_C(\theta) =$ constant. It further suggests that the actual distribution of skylight is less important than the solid angle subtended by the occulter.

B. Brightness Distribution inside a Shadow

The previous calculations showed the brightness at the center of the shadow, without regard to the distribution of light within the shadow. To compute the distribution, a number of factors must be considered (all relating to the solid angle of the occulter), as seen from both inside and outside the shadow. Figures 8–11 offer some insight into the situation. The sketches are in two dimensions, although the true situation is in three dimensions.

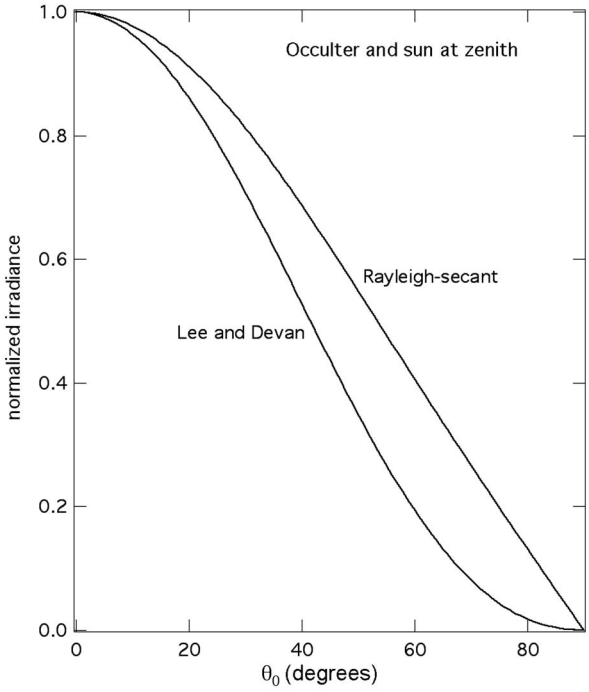

Fig. 7. Normalized comparison of the brightness of the center of the shadow for more realistic clear and overcast skies as a function of angular radius of the occulter [Eqs. (17) and (23)].

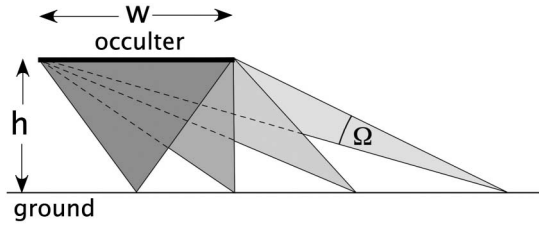

Fig. 8. Importance of the solid angle Ω of the occulter. The solid angle subtended by the occulter decreases with increasing distance from the center of the shadow. The gray shade of each triangle indicates the relative brightness of the shadow due to sky light.

Due to simple projection, the solid angle subtended by the occulter decreases with horizontal distance from the occulter's center [alternatively it decreases with increasing occulter zenith angle (Fig. 8)]. When the Sun is at the zenith, the shadow's brightness is symmetric about its center, but for a nonzenith sun the brightness is asymmetric (Fig. 9). Specifically, the side of the shadow closest to the Sun (proximal side) is darker than the side away from the Sun (distal side; Fig. 10). This is true because the solid angle Ω_p subtended by the occulter as seen from the proximal side is larger that it is from the distal side Ω_d. As a consequence, an observer on the proximal side of the shadow will receive less skylight (Fig. 10). As the occulter's solid angle varies across the shadow, so too does the corresponding amount of skylight that must be subtracted from the full sky (Fig. 11). The skylight distribution varies with elevation, further complicating the calculation. As it happens, calculating the solid angle subtended by a circular disk viewed obliquely is difficult if not impossible to do analytically [11–13]. While an arbitrary orthographic projection of a circular disk is an ellipse, the disk's projection is not the relevant quantity, but rather the solid angle it subtends as seen by an observer on the ground. For all these reasons, a complete computation of light distribution within a shadow is

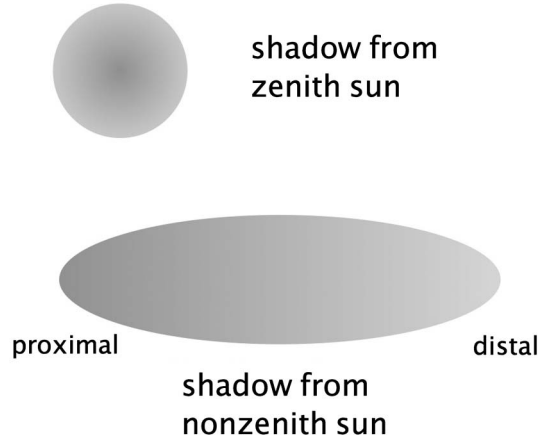

Fig. 9. A shadow cast by circular disk by a zenith sun is circular and symmetric about its center. It is also darkest at its center. A shadow cast by a nonzenith sun is brighter on its distal side than its proximal side.

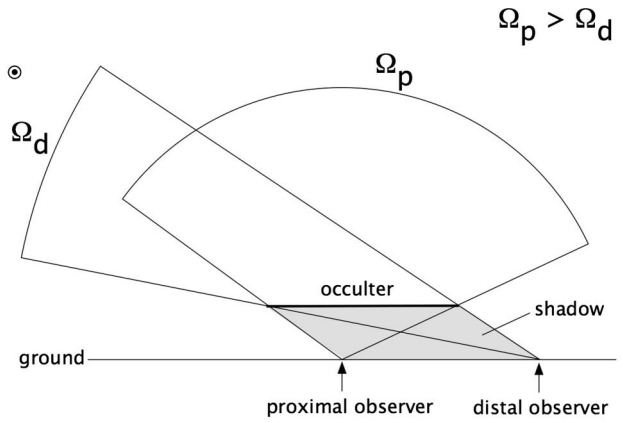

Fig. 10. The proximal edge is exposed to less of the sky than the distal side.

beyond easy reach. Therefore, we will numerically calculate the distribution using approximations.

To compute the solid angle Ω of the occulter from anywhere within the shadow, we approximated the disk as a grid of small unit squares (Fig. 12). The solid angle of each unit square was calculated by assuming that all parts of it were the same distance from the observer. Then, the individual solid angles were summed to get the total solid angle subtended by the occulter. Such calculations were done for a variety of observer locations and occulter heights.

Knowing Ω, however, does tell us the brightness across the shadow. We can, however, get a sense of the brightness by simply calculating the quantity F,

$$F = 2\pi - \Omega, \tag{24}$$

i.e., simply subtracting Ω from 2π, 2π being the brightness of the full sky [Eq. (5)]. Doing so makes the simplifying assumption that the sky is uniformly bright at all elevations. F is shown in Fig. 13 and captures many properties shown in Fig. 1.

The darkest shadows are from largest (lowest) occulters, i.e., those that subtend the largest solid angles and thus block the most light. As Ω decreases,

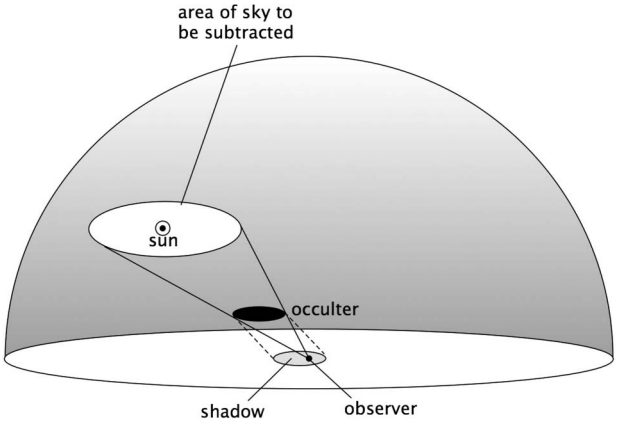

Fig. 11. The geometry of the nonzenith shadow is difficult to compute because of the variation of sky brightness and solid angle subtended from various locations on the ground.

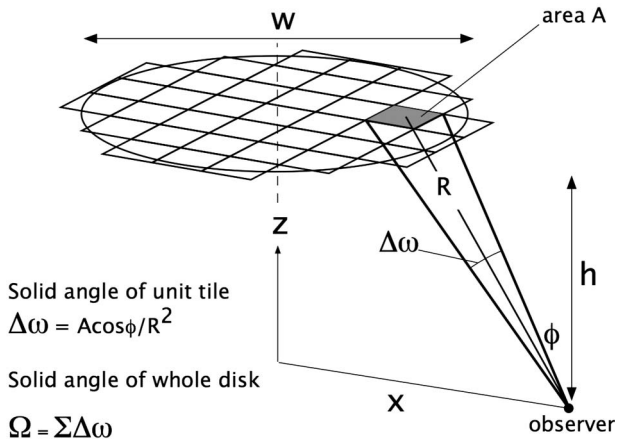

Fig. 12. Numerical approach to calculating the solid angle of the occulter. The circular disk was replaced by many smaller square tiles, each of whose solid angle was computed, then summed to get the approximate total solid angle Ω of the occulting disk.

the shadow brightens. All shadows are darkest at their centers and gradually brighten toward the edge. There are two limiting cases: (1) an occulter on the ground ($h = 0$, $\theta_0 = \pi/2$), whose shadow is completely and uniformly dark with a sharp edge; and (2) a very high occulter ($h = \infty$, $\Omega = 0$), whose shadow is of uniform brightness (2π) with no edge brightening. At all other values of h/w, the shadow is darkest at its center and brightens toward the edge, the effect being most pronounced when h/w is small.

Figure 13 also shows that the occulter influences the brightness outside the shadow ($x > 2$), because it still blocks part of the sky. As a result, even in the sunlit portions of the landscape, a nearby occulter decreases the total amount of light reaching the ground compared to what would otherwise reach the ground. The effect is most prominent for low occulters. The findings in Fig. 13 reinforce the observational result discussed in regard to Fig. 1. They also show that occulter solid angle is the most important factor

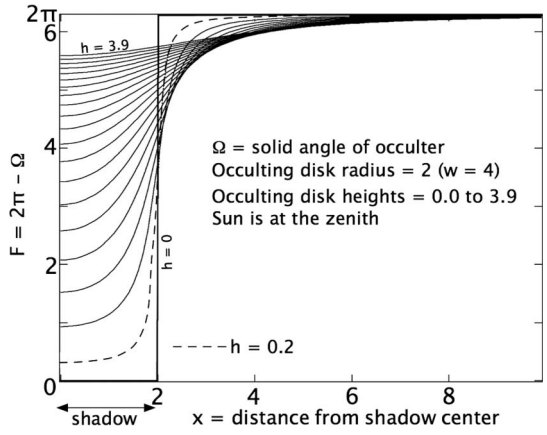

Fig. 13. Brightness proxy $F = 2\pi - \Omega$ for a circular black occulating disk as a function of distance from the center of the shadow. Note that F reveals the evidence of the blocked sky in the sunlit proportion of the scene adjacent to the shadow, i.e., F does not go to 2π for $x > 2$.

controlling shadow brightness. Thus, F becomes a proxy for brightness.

C. Brightness in Wells and Tunnels

Suppose that the occulting object is not an isolated object seen against the sky as previously discussed, but rather one that surrounds the observer and subtends almost 4π steradians. Such is the situation in wells and tunnels (Fig. 14). In this case, w is the diameter of the well and h is the depth of the observer. By assuming that the brightness is proportional to the solid angle Ω of the opening as seen from within the well, we eliminate the need for any knowledge about the illumination source.

From Eqs. (1) and (2),

$$\Omega = 2\pi(1-\cos\theta_0) = 2\pi(1-\cos(\tan^{-1}(w/2h))). \quad (25)$$

With two openings, a tunnel will obviously be twice as bright as a well, so we will just calculate the brightness as a function of depth in a well. We also assume that the walls of the well are nonreflective.

Figure 15 shows the brightness (solid angle) versus depth in a circular well whose diameter is unity. The maximum brightness occurs at $h = 0$, where $\Omega = 2\pi$ (again in units of steradians). Brightness drops off rapidly with depth, reaching about 10% of full brightness when $h = w$. After that, it asymptotically approaches total darkness as $h \to \infty$. A log – log plot (Fig. 15, inset) reveals that the brightness drops rapidly after the depth exceeds w. Note that the asymptotic slope of $\log \Omega / \log h$ is -2, which can be easily verified by expanding Eq. (25) in a power series.

3. Measurements of Shadows

A. High Sun

To measure the brightness distribution within shadows, we constructed a device mimicking the geometry of Fig. 4: a 30 cm diameter flat, black circular disk, suspended at various heights above a horizontal flat surface (Fig. 16). The location was on a ridge in the Santa Monica Mountains near Los Angeles, with a clear view of the entire sky. There was little in the way of trees or other objects that could reflect sunlight into the shadow, and the sky was visible down to an altitude of 3° or less in any direction. Measurements were made on 26 June 2013 when the Sun's altitude was 77°, near but not at the zenith. Photographs were taken of the disk's shadow for various heights and scanned in the same way as shown in Fig. 1. We included calibration cards in each photo but did not convert the pixel values to true relative intensity. Red-green-blue (RGB) values are good proxies for relative intensities because tests of the camera showed a monotonic relation between RGB and relative brightness.

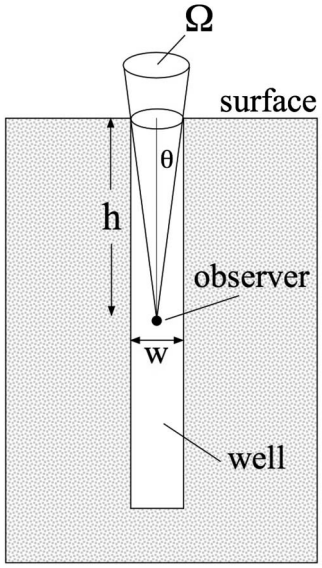

Fig. 14. Optical geometry of a well.

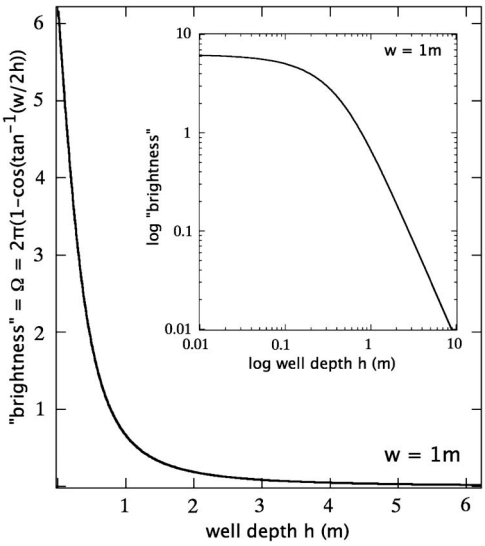

Fig. 15. Brightness inside a well as a function of observer depth. Inset, logarithmic plot.

Figure 17 shows three line scans through shadows where the disk height was varied. Owing to slightly different camera exposures, the three plots have been scaled by a small amount to match the upper and lower portions of the scans. This aids in comparison of shape but hides another fundamental fact about shadows mentioned previously: the larger the angle subtended by the occulter, the darker the shadow, as Fig. 13 clearly shows. As previously, blue pixels are the brightest and red ones are the faintest.

The line scans show the brightness distribution across the shadow for three values of h/w. These qualitatively agree with the predictions of Section 2 (Fig. 13): occulters closer to the ground produce greater brightness variations across the shadow. Two other aspects of Fig. 17 are worth noting. The influence of the occulter in the sunlit portion is most evident when the occulter is low ($h/w = 0.17$), where the brightness increases away from the shadow. The steepness of the shadow/sunlight boundary decreases as h/w increases. This is the result of a wider penumbra.

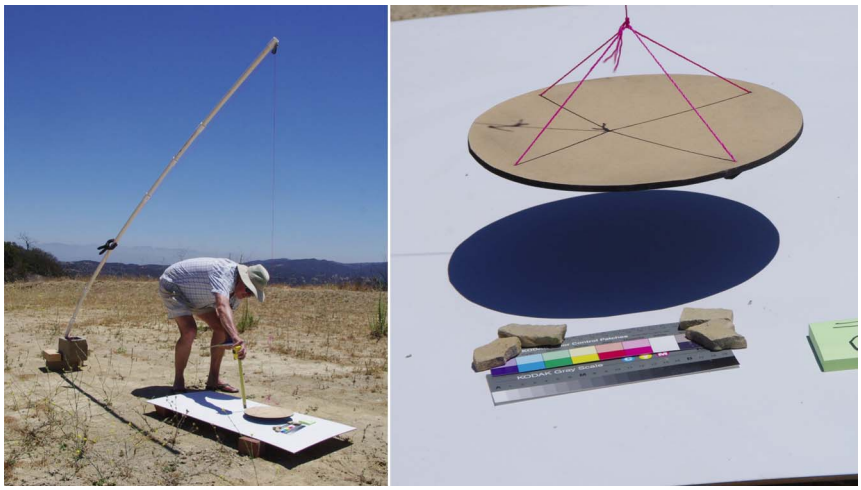

Fig. 16. Left, a shadow making apparatus was constructed to mimic the conditions in Fig. 4. A black circular black disk was suspended at various heights from a slender pole on a high mountain ridge on a clear day when the Sun was high in the sky, although not precisely at the zenith. Right, shadows were photographed and scanned (see Fig. 17).

B. Low Sun

When the Sun is low and shadows long, shadows are offset horizontally away from the Sun. The shifted placement (relative to the center of the occulter) results in an asymmetric brightness distribution across the shadow. Figure 18 shows a photograph of such a clear-sky situation, with a 12 cm diameter black, circular disk, held 2 cm above a diffuse white horizontal surface. The Sun was at an elevation was 31° in the northwestern sky. Although illumination conditions were not ideal because trees and buildings blocked some of the eastern sky, the effect shown in Figs. 9 and 10 is nonetheless obvious: the proximal edge is darker than the distal edge.

4. Reconciling Theory with Measurements

There are at least two aspects of the observations in Fig. 17 that Fig. 13 does not reproduce. (1) Calculations show F (Fig. 13) to be near zero at the center of shadows for low occulters, yet measurements show that the centers of shadows have significant brightness. (2) The edges of shadows in Fig. 17 are quite sharp, while those in Fig. 13 are smooth and continuous across the shadow/sunlit boundary. Both discrepancies are a consequence of using $F = 2\pi - \Omega$ as a substitute for brightness. F was derived from solid angles, not from actual calculation of brightness. To bring theory closer to measurement, we simply need to add a constant offset to F to account for skylight reaching the shadow. This would not, however, correct the disparity of sharp edges, because the solid angles are continuous across the shadow/sunlit boundary.

Theory also predicts that the darkest part of the shadow in Fig. 18 should be directly beneath the center of the occulter (as it is in Fig. 17), but this is not the case for the observations shown in Fig. 18. The darkest part is to the right (more distal) of the center of the disk. We believe that this is because the sky is brighter in the direction of the Sun (due to forward scattering by aerosols) than it is away from it. We believe that it is the enhanced brightness of the sky (near the low sun) that raises the brightness of the proximal part of the shadow.

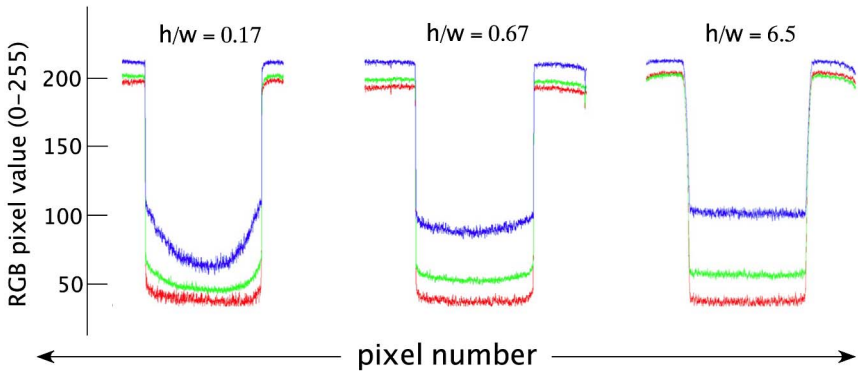

Fig. 17. Three RGB scans through three shadows cast by the occulter at various heights. The Sun was near the zenith. The shadow is blue and darkest at its center, i.e., directly beneath the center of the occulter. For a low occulter ($h/w = 0.17$, left scan) the central shadow is quite dark, while for a high occulter ($h/w = 6.5$, right scan) the shadow is nearly the same brightness throughout. These results confirm the predictions made in Section 2.B.

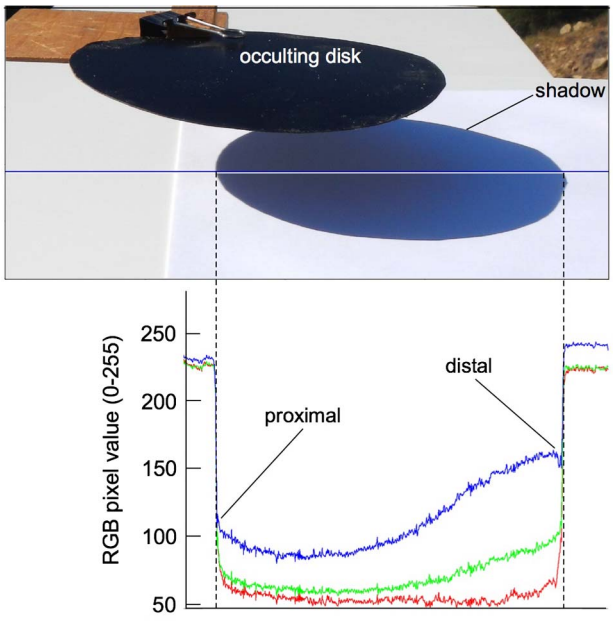

Fig. 18. RGB scan through a shadow cast when the Sun was at an altitude of 30°. Note that the proximal side of the shadow (left) is darker than the distal side (right). Sky conditions were not ideal. There were some thin clouds to the west (left), and much of the horizon to the east (right) was blocked by trees and buildings. As a result, the darkest part of the shadow is not precisely under the center of the occulter, as would be the case for a clear, unobstructed sky as indicated in Fig. 9.

5. Influence of the Aureole

The aureole is a bright glow around the Sun, caused by forward scattering of large aerosol particles (10–1000 μm), usually dust, thin clouds, or pollen. Near sea level or in the planetary boundary layer, the aureole is always present. Even on high mountains, it is rarely absent (Fig. 19). The aureole therefore brightens the periphery of shadows in proportion to its brightness and radial extent. This adds a term to Eq. (3), representing a localized brightness enhancement. Indeed, having been taken in the planetary boundary layer, Figs. 1, 16, and 18 must have an aureole component.

The importance of aureoles to shadow illumination is easily argued. Assume the sky subtends 2π sr and is of unit brightness. A 5° diameter aureole subtends about 0.006 sr, so on average would only have to be $2\pi/0.006 \approx 1000$ times as bright as a Rayleigh atmosphere to significantly affect the shadow's periphery. Aureoles can be much brighter than this, as Fig. 20 shows.

Two brightness profiles of the aureole were measured, on a clear day and a hazy day, in [14] (Fig. 20). On the clear day, the aureole (near 0.4° from solar center) was about 1000 times fainter than the disk of the Sun, but on the hazy day (when the Sun's brightness was attenuated by about a factor of 2), the aureole was much brighter, only about 100 times fainter than the solar disk.

The aureole modifies the sky's brightness distribution and might render the $\sec\theta$ approximation [Eq. (3)] locally incomplete. However, for an optically thin aerosol layer, we suppose that its contribution can be modeled by adding an additional term to Eq. (3) to represent the aureole's glow.

6. Shadows from Clouds with Optically Thin Edges

A fascinating suggestion was made in [15]. By modeling a scene containing clouds with optically thin edges, they predicted that the periphery of cloud shadows should have bright rings around them (Fig. 21). Their argument was as follows. An optically thick cloud will cast a dark shadow. At its optically thin edges, however, forward scattering by water droplets will distribute sunlight across the geometrical shadow boundary. The main effect is to add additional light to the shadow edge (Fig. 22). Therefore, there should be a thin, bright band of light around the cloud's shadow. More recently, [16] has strengthened the case for "enhanced illumination" near cloud shadow boundaries.

7. Summary and Conclusions

We have investigated shadows cast by a circular disk both theoretically and experimentally and found them to be in qualitative (and in some cases quantitative) agreement. We began by making a simple but surprising observation (Fig. 1) that showed that the presence of an occulting object affects the brightness in the sun-illuminated portions of the ground. We computed the brightness at the center of the shadow as a function of the occulter's apparent size on the sky, and then showed how the brightness varies across it. The brightness in wells as a function f depth was also calculated. We then made measurements of actual shadows and found them to be in agreement with theory. For shadows cast by an off-zenith occulter, the proximal side of the shadow is

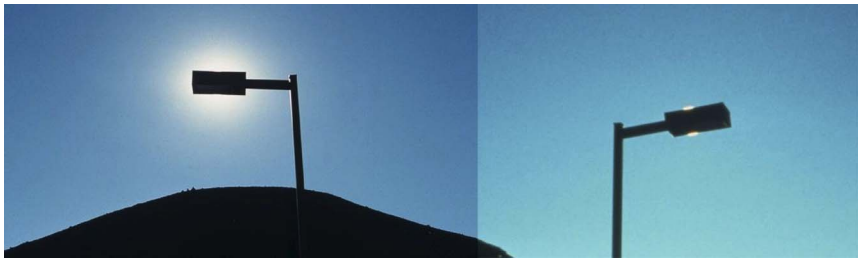

Fig. 19. The bright glow around the Sun (blocked by the street light) is the aureole and is almost always present due to forward scattering by particulates (left). On one exceptionally clear day on Mauna Kea, the aureole was undetectable (right).

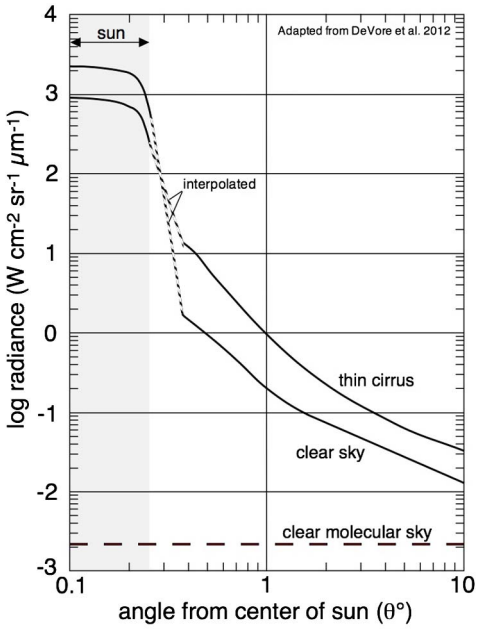

Fig. 20. Brightness of two aureoles by [14]. Aureole brightness can be 10^3–10^5 brighter than the pure molecular sky.

darker than the distal side. The influence of the aureole and how it affects the periphery of the shadow were also discussed.

At this point, one might say, "Well, of course shadows are darkest at their centers," or other such sentiments, as though nothing new was found (or the results were common sense and unremarkable). Perhaps, having now explained the properties of shadows, the results do indeed seem rather unsurprising. But Galileo knew that new findings often seem obvious in retrospect:

> "All truths are easy to understand once they are discovered; the point is to discover them."

This quote has been widely attributed to Galileo, but it is actually a paraphrasing of an exchange between two interlocutors in [17]:

Salviati: "Now you see how easy it is to understand."

Fig. 21. Model prediction of bright edges to cloud shadows [15,16].

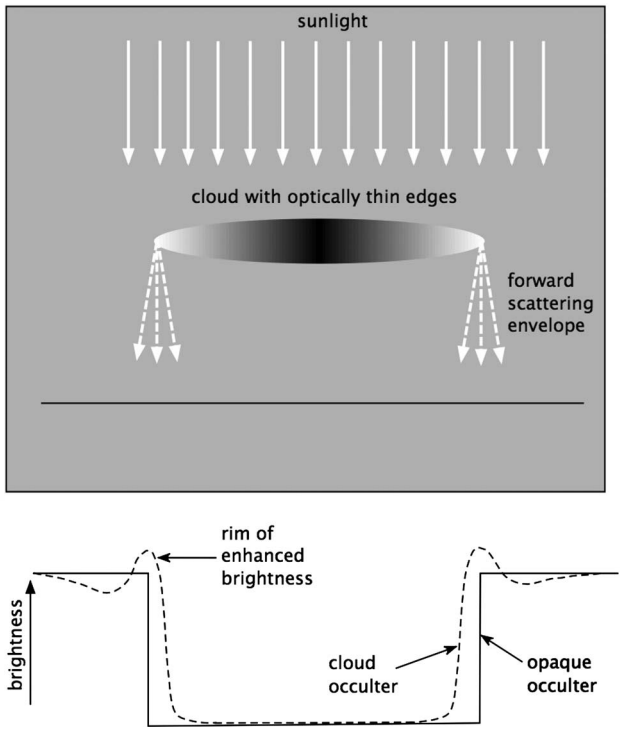

Fig. 22. The bright edges of cloud shadows could result from forward scattering through the optically thin edges of the cloud. The effect has not been reported for real clouds and perhaps has never been sought.

Sagrego: "So are all truths, once they are discovered. The point is in being able to discover them." [18].

The author would like to thank James Lock for reviewing the theoretical analysis and David Dearborn for performing the calculation in Fig. 13. We appreciate many useful discussions with Bill Livingston about shadows. Many substantive suggestions were made by two anonymous reviewers, and we acknowledge with gratitude their contributions to the paper.

References and Notes

1. The names form, space, and cast are not universally used. Three other analogous terms are body (or attached), volume, and ground, respectively.
2. M. Agrawala, R. Ramamoorthi, A. Heirich, and L. Moll, "Efficient image-based methods for rendering soft shadows," in *Proceedings of the 27th Annual Conference on Computer Graphics and Interactive Techniques (SIGGRAPH '00)* (2000), pp. 375–380.
3. J. Gurney, *Color and Light: A Guide for the Realist Painter* (Andrews-McNeal, 2010).
4. U. Assarsson, "A real-time soft shadow volume algorithm," Technical Report No. 18D (School of Computer Science and Engineering, Chalmers University of Technology, 2003), available at http://fileadmin.cs.lth.se/graphics/research/shadows/ulf_thesis_lores.pdf.
5. I. Y. Sato and K. Ikeuchi, "Illumination distribution from brightness in shadows: adaptive estimation of illumination distribution with unknown reflectance properties in shadow regions," in *Proceedings of the Seventh IEEE International Conference Computer Vision* (IEEE, 1999), Vol. **2**, pp. 875–882.
6. T. Kim and K. Hong, "A practical approach for estimating illumination distribution from shadows using a single image," Int. J. Imag. Syst. Technol. **15**, 143–154 (2005).

7. T. Kim and K.-S. Hong, "A practical single image based approach for estimating illumination distribution from shadows," in *Tenth IEEE International Conference on Computer Vision (ICCV '05)* (IEEE, 2005), Vol. **1**, pp. 266–271.
8. R. L. Lee, Jr. and D. E. Devan, "Observed brightness distributions in overcast skies," Appl. Opt. **47**, H116–H127 (2008).
9. P. Moon and D. E. Spencer, "Illumination from a non-uniform sky," Illum. Eng. **37**, 707–726 (1942).
10. S. Fritz, "Illuminance and luminance under overcast skies," J. Opt. Soc. Am. **45**, 820–825 (1955).
11. R. P. Gardner and A. Carnesale, "The solid angle subtended at a point by a circular disk," Nucl. Instrum. Methods **73**, 228–230 (1969).
12. M. J. Prata, "Analytical calculation of the solid angle subtended by a circular disc detector at a point cosine source," Nucl. Instrum. Methods Phys. Res. A **521**, 576–585 (2004).
13. F. Paxton, "Solid angle calculation for a circular disk," Rev. Sci. Instrum. **30**, 254–258 (1959).
14. J. G. DeVore, A. T. Stair, A. Le Page, D. Rall, J. Atkinson, D. Villanucci, S. A. Rappaport, P. C. Joss, and R. A. McClatchey, "Retrieving properties of thin clouds from solar aureole measurements," J. Atmos. Ocean. Technol. **26**, 2531–2548 (2012).
15. A. Berk and S. C. Richtsmeier, "Monte Carlo hyperspectral scene simulator," in *25th Annual Review of Atmospheric Transmission Models*, 24 June 2002 (Spectral Sciences, 2002), pp. 24–27.
16. R. L. Sundberg, S. Richtsmeier, and S. Adler-Golden, "Influence of broken cloud fields on reflectance retrievals," Proc. SPIE **9242**, 924208 (2014).
17. G. Galilei, *Dialogue Concerning the Two Chief World Systems* (1632).
18. B. Sheppard, *The Logic of Infinity* (Cambridge University, 2014), p. 398.